Zeeman Field-Induced Two-Dimensional Weyl Semimetal Phase in Cadmium Arsenide

Binghao Guo[1], Wangqian Miao[1], Victor Huang[1], Alexander C. Lygo,[1] Xi Dai[1,2] and Susanne Stemmer[1,*]

[1]*Materials Department, University of California, Santa Barbara, California 93106-5050, USA*
[2]*Department of Physics, Hong Kong University of Science and Technology, Hong Kong, China*

We report a topological phase transition in quantum-confined cadmium arsenide (Cd_3As_2) thin films under an in-plane Zeeman field when the Fermi level is tuned into the topological gap via an electric field. Symmetry considerations in this case predict the appearance of a two-dimensional Weyl semimetal (2D WSM), with a pair of Weyl nodes of opposite chirality at charge neutrality that are protected by space-time inversion (C_2T) symmetry. We show that the 2D WSM phase displays unique transport signatures, including saturated resistivities on the order of h/e^2 that persist over a range of in-plane magnetic fields. Moreover, applying a small out-of-plane magnetic field, while keeping the in-plane field within the stability range of the 2D WSM phase, gives rise to a well-developed odd integer quantum Hall effect, characteristic of degenerate, massive Weyl fermions. A minimal four-band $k \cdot p$ model of Cd_3As_2, which incorporates first-principles effective g factors, qualitatively explains our findings.

Topologically nontrivial states of matter in two-dimensions (2D) have distinct advantages over their three-dimensional counterparts, as they can be readily manipulated by electric and/or magnetic fields, epitaxial strain, and proximity effects. A prime example is the quantum spin Hall insulator, known also as a 2D topological insulator (2D TI) [1,2], which supports helical edge modes inside a bulk energy gap in the presence of time-reversal symmetry. When subjected to in-plane magnetization, 2D TIs are predicted to give rise to an even richer variety of electronic states. These include quantum anomalous Hall insulators [3–6], density-wave states [7], as well as 2D (topological) semimetals [4,5,8]. While there exists a considerable amount of literature studying 2D TIs in out-of-plane magnetic fields (see, e.g., Refs. [9,10] and references cited therein), in-plane magnetization-induced phases have only recently been investigated [11–13]. As a result, the underlying nature of the observed transitions remains less clear. In principle, an in-plane magnetization can be supplied using magnetic dopants [5], or directly by an external magnetic field B_{ip} that is oriented in the plane of the 2D system. The latter approach offers magnetic field tunability and is furthermore not limited to magnetic materials that require careful control of impurity concentrations and interactions. The main effect of B_{ip} is to modify the electronic structure of 2D electronic systems via Zeeman coupling, $\Delta E_Z \sim g\mu_B B_{ip}$, where the g factor is sample and material specific, and μ_B is the Bohr magneton.

In narrow gap semiconductors, a class that includes all experimentally observed 2D TIs, an in-plane Zeeman field may be sufficient to modify the topology of the Fermi surface. Several theoretical studies [4,8,14–16] have predicted that B_{ip} can close the zero-field gap of a 2D TI and thereby drive the system into a metallic phase, when the holelike and electronlike subbands overlap in momentum space. Topological classification of this predicted (semi)metallic phase remains ambiguous both experimentally and theoretically. Early transport data from inverted HgTe quantum wells suggested a conventional metal, based on observing a suppression of the local (and nonlocal) resistances in the diffusive transport regime [11].

In this Letter, we study the evolution of the recently reported [17] 2D TI phase of epitaxial cadmium arsenide (Cd_3As_2) thin films under in-plane and tilted magnetic fields and identify the gapless phase as a 2D Weyl semimetal (WSM) with two valleys (nodes). A combined C_2T symmetry protects the 2D WSM from opening an energy gap across the entire Brillouin zone, up to at least $B_{ip} \sim 14$ T. Our conclusions are based on the following: (1) once the Fermi level is tuned to the charge neutrality point, closing of the inverted gap leads to a state with a saturated resistivity on the order of h/e^2, which spans a range of in-plane magnetic fields; (2) a well-developed odd integer quantum Hall (QH) effect appears when a small out-of-plane magnetic field is applied along with the in-plane field, a direct consequence of chiral zeroth Landau levels contributed by 2D Weyl nodes; and (3) experimental observations are consistent with a four-band $k \cdot p$ model of confined Cd_3As_2 films [18,19] under an in-plane magnetic field and considering effective g factors for Cd_3As_2 thin films implemented within first-principles codes [20,21].

We begin by discussing expectations from symmetry considerations for a 2D TI Cd_3As_2 thin film in an in-plane

magnetic field. In the absence of a magnetic field, Cd_3As_2 thin films possess $4/mmm$ point group and time reversal (T) symmetries [22]. Under an in-plane field, the symmetry reduces to the magnetic point group $2'/m'$, which contains the symmetry operators E, C_2T, M_zT, and inversion. As discussed in Ref. [23], C_2T symmetry eliminates one of the three Pauli matrices for the Hamiltonian at any specific k point in the 2D Brillouin zone. This leads to a 2D WSM within a finite phase region when the band gap is inverted by a tunable parameter (in the present case, the in-plane field strength). The significance of C_2T symmetry to the local stability of the Weyl nodes against perturbations has also been discussed extensively in Ref. [24]. Our computational results for the quantum well subbands confirm this symmetry analysis, as discussed next.

Figure 1(a) shows the dispersion in the E-k_y plane computed for an 18 nm film at $B_{ip} = 10$ T, obtained from a symmetry-invariant $k \cdot p$ Hamiltonian [25] for Cd_3As_2. The effective model parameters, and in particular the in-plane g factors, are calculated by quasidegenerate perturbation theory [26,27], implemented in a first-principles code [20,21]. As described in detail in Ref. [21] and in the Supplemental Materials [28], to obtain an accurate theoretical treatment of the magnitude of B_{ip} effects, our approach involves further renormalizing the g factors of Cd_3As_2 thin films, known to be large in the bulk (>20 [32,33]), to account for the effects of quantum confinement. The dominating in-plane g factor (g_{1p}; see Ref. [28]) is found to be ~12 in the bulk and ~13 for an 18-nm-thin film. The key result of this calculation is an isolated pair of Weyl nodes at the Fermi level, which are split along the direction perpendicular to the applied field. The results imply that their low-energy physics can be accessed at lab-scale magnetic fields. The degeneracy of the two Weyl nodes is furthermore guaranteed by bulk inversion symmetry present in Cd_3As_2 thin films [22,34,35]. Without a Zeeman field, the 18 nm film is a 2D TI, with doubly degenerate subbands [Fig. 1(b)], consistent with our previous experimental results [17]. A calculated phase diagram of the band gap as a function of the in-plane field and the film thickness is shown in Fig. 1(c). The predicted thickness range for the 2D TI phase at zero field is in excellent agreement with our previous experiments [17]. We now turn to the experiments.

Transport measurements were carried out using top-gated Hall bars fabricated from high-mobility (001) Cd_3As_2 films, grown by molecular beam epitaxy to thicknesses of 18 and 22 nm, respectively, on nearly lattice-matched buffer layers of $Al_{0.45}In_{0.55}Sb$, supported by (001) GaSb substrates [36]. Both film thicknesses fall within the 2D TI ("inverted") regime [17]. High-resolution x-ray reciprocal space maps, taken around the buffer 224 Bragg reflection, are shown in Ref. [28]. Data from four-point resistance measurements using low-frequency lock-in techniques are presented as two-dimensional resistivities or conductivities. All data were recorded at $T = 2$ K, unless
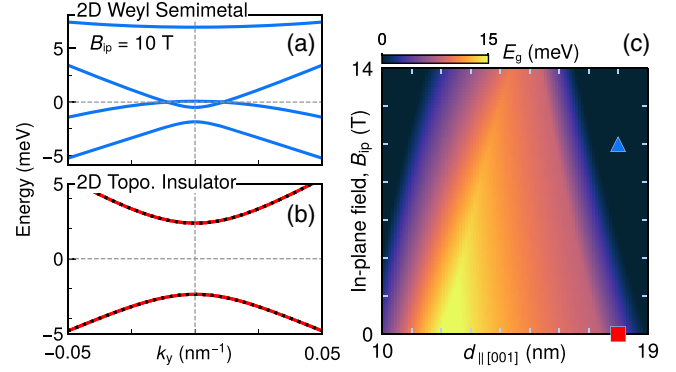

FIG. 1. 2D Weyl semimetal phase induced by a Zeeman field in confined Cd_3As_2. (a) Dispersion of the semimetal phase with two Weyl nodes located at the Fermi level ($E = 0$ meV, dashed line). The 4 bands are spin resolved. For the $k \cdot p$ slab calculation, Cd_3As_2 has a thickness $d = 18$ nm along [001] with an in-plane field $B_{ip} = 10$ T. (b) Dispersion of the topological insulator phase with no external magnetic field. The spin-degenerate bands are drawn as dashed red lines. (b) Phase diagram of the Γ-point energy gap in the B_{ip}-d parameter space. The thickness range corresponds to the band inversion regime. Blue triangle, 2D WSM; red square, 2D TI.

stated otherwise. With no gate voltage applied, the 18 nm film had a low-field Hall mobility $\mu = 2.8 \times 10^4$ cm^2 V^{-1} s^{-1} at an electron density $n_{2D} = 3.6 \times 10^{11}$ cm^{-2}, while the 22 nm film had $\mu = 1.7 \times 10^4$ cm^2 V^{-1} s^{-1} at $n_{2D} = 5.5 \times 10^{11}$ cm^{-2}. For measurements with an additional out-of-plane field component B_{oop}, the total field B_{tot} was fixed, while the samples were rotated *in situ* (for the angular alignment procedure, see Ref. [28]). The angle θ relative to the sample normal ($+z$ direction) was defined such that $\theta = 90°$ corresponds to the field positioned completely in plane. The fields in other cases are related to each other by $B_{oop} = B_{tot} \cos\theta$ and $B_{ip} = B_{tot} \sin\theta$.

Before we discuss the unusual nature of the in-plane results, we show, as an important point of comparison, the case with the magnetic field oriented fully out of plane. Figure 2(a) shows the longitudinal conductivity $\sigma_{xx}(B_{oop})$, measured on the 18 nm sample as a function of top-gate voltage (V_g). A modified gate voltage scale, $V_g - V_{CNP}$, is used to later aid comparison of films with slightly different as-grown carrier densities, where V_{CNP} is the voltage corresponding to a global maximum in $\rho_{xx}(B_{tot} = 0)$. The evolution of subband Landau levels (LLs), and, in particular, the crossing of two $n = 0$ LLs, where n is the LL index, is characteristic of the previously reported subband inversion in Cd_3As_2 [17]. A specific point to note is that spin or "isoparity" degeneracy (when spin is not a conserved quantum number [37]) is lifted at any finite B_{oop} for $n > 0$ LLs [17,38], as evidenced by the appearance of completely developed, *even and odd* integer quantum Hall states at the same low $B_{oop} \sim 1.5$ T. This point will become important later, because it clearly distinguishes the
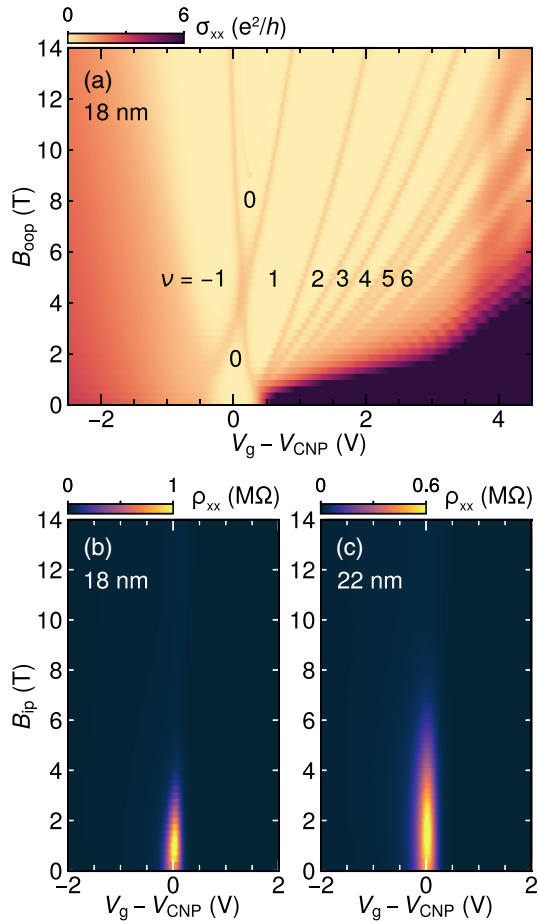
FIG. 2. Out-of-plane and in-plane magnetotransport. (a) Longitudinal conductivity σ_{xx} as a function of the out-of-plane field B_{oop} and the scaled (relative to V_{CNP}) top-gate voltage for the 18 nm sample (device, hb1). Quantum Hall plateau regions are indexed by their filling factor ν up to 6. The measured voltage V_g is offset by V_{CNP}, which corresponds to the charge neutrality condition defined in the main text. (b) Longitudinal resistivity ρ_{xx} as a function of the in-plane field B_{ip} and the top-gate voltage for the 18 nm Cd_3As_2 sample (device, hb1). The same is shown in (c) for the 22 nm sample. $V_{CNP} = -1.35$ V for the 18 nm sample, $V_{CNP} = -1.165$ V for the 22 nm sample. Measurements were done at $T = 2$ K in the transverse configuration.
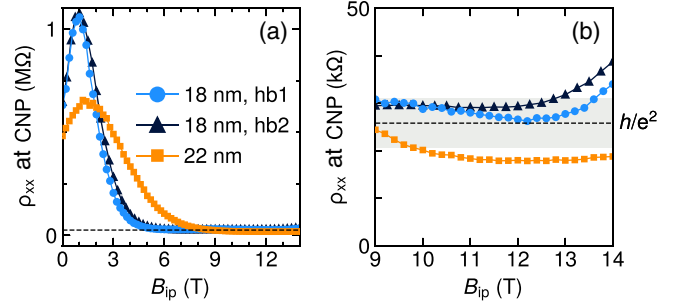

FIG. 3. Suppressed resistivity on the order of h/e^2 in the WSM phase. (a) Extracted ρ_{xx} at the charge neutrality condition as a function of B_{ip} for the 18 nm sample (devices hb1 and hb2 are on the same sample) and the 22 nm sample. (b) Close-up of the $B_{ip} > 9$ T region for the data in (a). Shading indicates a $\pm 20\%$ interval around the resistance quantum $h/e^2 \approx 25.81$ kΩ (dashed line).

topological phases in B_{oop} and B_{ip}. A higher-energy conduction subband contributes an additional set of LLs at 4 V, outside the low-energy window of interest for in-plane experiments, and we do not discuss it in this study.

Next, we examine the same device with the magnetic field fully in plane. In Fig. 2(b), we show the longitudinal resistivity $\rho_{xx}(B_{ip})$ of the 18 nm sample as a function of $V_g - V_{CNP}$, which tunes the 2D carrier system from n- to p-type transport regimes. Resistivity traces at constant B_{ip} peak around 0 V, but the peak magnitude shows a non-monotonic evolution with increasing B_{ip}: the peak resistivity increases rapidly at low fields, followed by a sharp drop past ~1 T. The 22 nm Cd_3As_2 film, which lies at the other end of the thickness range for the inverted (2D TI) phase, demonstrates similar behavior, as shown in Fig. 2(c). Our results are qualitatively similar to that of inverted (001) HgTe quantum wells at comparable magnitudes of B_{ip} [12]. Representative traces of $\rho_{xx}(V_g - V_{CNP})$ at fixed B_{ip} are provided in Ref. [28].

In Fig. 3(a), we extract the peak resistivity under B_{ip} from the two inverted samples to visualize the band gap closing under large Zeeman fields. The transition point, where $d\rho_{xx}/dB_{ip}$ goes to zero, is ~1 T in both samples. Beyond this transition point, the rate of gap closing is greater in the 18 nm sample than in the 22 nm sample. The gap is consequently closed at a higher field in the 22 nm sample. In the gapless region, shown in Fig. 3(b), both samples exhibit resistivities on the order of the resistance quantum h/e^2, with the 22 nm sample showing slightly lower values (~0.8 h/e^2). For the 18 nm sample, a >90% reduction of resistivity as compared to zero-field values is observed, i.e., giant negative magnetoresistance. Also, while the 22 nm sample shows a saturated resistivity [Fig. 3(b)], the 18 nm sample has additional structure in the gapless region that is qualitatively reproducible between devices on the same film (hb1 vs. hb2) and that requires further investigation beyond the present study. We note that a resistivity value near h/e^2 is reasonably close to what is expected for 2D Dirac/Weyl systems [39,40]. The gap closing and transition to a semimetal phase is further confirmed by the temperature dependence of the resistivities; see Ref. [28]. The wide range of B_{ip}, within which the gapless phase is found, is one of the key experimental results, because it is consistent with the predicted wide stability range of the Zeeman field-induced 2D WSM phase, as discussed earlier.

To further characterize the nature of the 2D semimetal, we focus on its QH effect when both in-plane and out-of-plane magnetic fields are present. This is accomplished by tilting the film ($\theta < 90°$), while keeping B_{tot} constant.
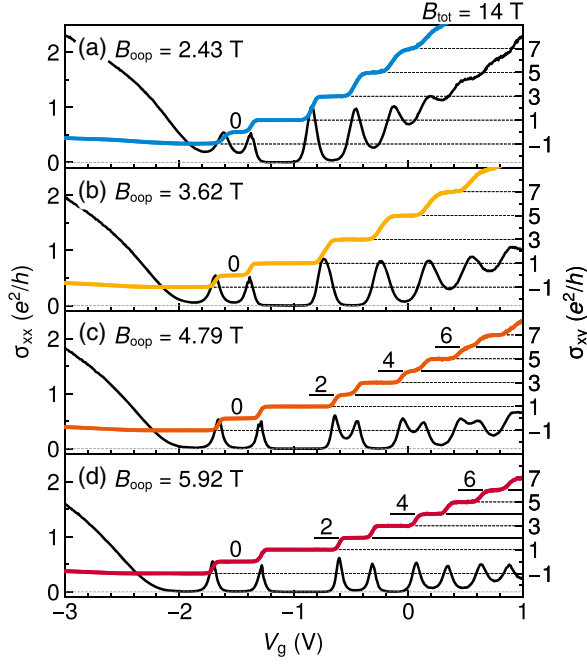
FIG. 4. Odd integer quantum Hall effect and valley splitting. (a) Longitudinal and Hall conductivities, σ_{xx} and σ_{xy}, as a function top-gate voltage for a fixed $B_{oop} = 2.43$ T. The same is shown in (b) for $B_{oop} = 3.62$ T, in (c) for $B_{oop} = 4.79$ T, and in (d) for $B_{oop} = 5.92$ T. The total magnetic field $B_{tot} = 14$ T, which is fixed, and $B_{ip} > 12.5$ T in the four cases. σ_{xy} is drawn with different colors and σ_{xx} is drawn in black. Dashed black lines, $\nu =$ odd integers. Bold lines, $\nu =$ even integers, which are also labeled. The $\sigma_{xy} = 0$ plateaus are labeled separately.

The out-of-plane component will gap the C_2T-symmetric Weyl nodes, thus allowing us to investigate the 2D WSM's QH effect. We study the 18 nm sample, which enters the gapless phase at lower B_{ip}. In Fig. 4, we present sets of $\sigma_{xx}(V_g)$ and $\sigma_{xy}(V_g)$ traces, one set for each of four tilt angles, 80°, 75°, 70°, and 65° from Figs. 4(a)–4(d), at $B_{tot} = 14$ T. The corresponding B_{oop} values are 2.43, 3.62, 4.79, and 5.92 T with an uncertainty of ±0.05 T [28]. B_{ip} is greater than 12.5 T in all cases so that the sample remains in the B_{ip} range of the gapless phase.

We make two main observations regarding the QH effects seen in Fig. 4. First, using the fact that a $\sigma_{xy} = 0$ plateau ($\nu = 0$) is present in all tilt cases and connects to $\nu = \pm 1$ plateaus, we deduce that the two zeroth LLs are spin resolved; otherwise their contribution to the filling factor sequence would be in increments of two (or higher if there are other degeneracies). This is also consistent with their dispersion in B_{oop} up to 5.92 T, which causes the $\sigma_{xy} = 0$ plateau to continuously widen on the V_g scale. We contrast the behavior in the gapless phase with the B_{oop} LL spectrum shown in Fig. 2(a), where the $\sigma_{xy} = 0$ plateau narrows down until it vanishes near 5 T when the two zeroth LLs meet.

Second, the LLs with $|n| \geq 1$ give rise to an *odd integer* sequence of filling factors. At $B_{oop} \leq 3.62$ T, as shown in Figs. 4(a) and 4(b), in addition to $\nu = \pm 1$, σ_{xy} plateaus at $\nu = 3$, 5, and 7 are most prominent, but additional minima in $\sigma_{xx}(V_g)$ appear at electron densities corresponding to $\nu = 9$ and $\nu = 11$. We therefore conclude that higher order LLs are twofold degenerate when B_{oop} is small, a remarkable contrast to our findings when there is no in-plane field [Fig. 2(a)]. Together with the spin-resolved zeroth LLs discussed earlier, this odd-integer-only sequence suggests the existence of a pair of massive Weyl fermions, whose filling factors are expected to follow a $2(n + 1/2)$ sequence [41,42]. The two Chern insulators, one that develops from the 2D TI and the other from the 2D WSM state, are thus easily distinguished at low out-of-plane fields. In Ref. [28] we provide another 32 sets of conductivity traces, acquired at lower B_{tot} values (down to 10 T) and using the same four tilt angles, showing that the results in Fig. 4 continue to hold for the full range of the gapless phase.

The key features in the data can be explained within a minimal model for a gapped 2D Weyl semimetal under a Zeeman field. For a Weyl point in a single valley (K^+), the Hamiltonian under a quantizing magnetic field is well studied and can be written as

$$H_{K^+} = \begin{pmatrix} \Delta & v_F \Pi^\dagger \\ v_F \Pi & -\Delta \end{pmatrix}, \qquad (1)$$

$$H_{K^+} = \begin{pmatrix} g_z B_z & v_F[(\hbar k_x + eB_z y) - \hbar \nabla_y] \\ v_F[(\hbar k_x + eB_z y) + \hbar \nabla_y] & -g_z B_z \end{pmatrix},$$
$$(2)$$

where Zeeman coupling is included as a mass term $\Delta = g_z B_z = g_z B_{oop}$, g_z is an out-of-plane g factor, and v_F is an isotropic Fermi velocity. The energy eigenvalue for the $n^+ = 0$ Landau level is directly obtained as $E(n^+ = 0) = g_z B_z$, and the higher order LLs ($|n^+| \geq 1$) are $E(|n^+| \geq 1) = \pm \sqrt{|n_+| \hbar^2 \omega_0^2 + \Delta^2}$, where $\omega_0 = \sqrt{2} v_F / l_B$ and $l_B = \sqrt{\hbar/(eB_{oop})}$ is the magnetic length. The valley with opposite chirality (K^-) shares the same solutions for higher order LLs, but the $n^- = 0$ Landau level experiences a sign change, with an eigenvalue of $E(n^- = 0) = -g_z B_z$. This model of the 2D WSM readily explains the observed twofold degeneracy of higher order LLs as coming from an expected valley degree of freedom, while the absence of any degeneracy for the two zeroth LLs are accounted for by their chirality. By only keeping up to linear terms in momentum, however, the model cannot describe the lifting of the valley degeneracy at large B_{oop}, seen in Figs. 4(c) and 4(d), which creates additional σ_{xy} plateaus at even filling factors of 2, 4, and 6. We note that the lifting of the degeneracy is not likely due to a Lifshitz transition at high

V_g, since all data in Fig. 4 span the same V_g range. This observation should motivate future theoretical work toward a more complete description. As in conventional semiconductor systems, such as AlAs quantum wells, lifting of valley degeneracy may originate from electron correlation effects [43,44].

To conclude, we comment on the observation of such a well-developed odd integer QH effect in a topological material. Odd integer QH sequences have long been sought after in three-dimensional (3D) TIs subjected to perpendicular magnetic fields [45–50], because they provide a clear transport signature of the Dirac fermions on their surfaces. In 3D TIs, this odd integer QH effect is typically thwarted by the energy mismatch between the 2D Dirac fermions on the top and bottom surfaces and the continued conduction of the side surfaces in a perpendicular magnetic field [51].

Finally, we note that the ideal 2D WSM reported here is particularly noteworthy, given the rarity of ideal WSMs in 3D [34]. Moreover, as discussed in this Letter, the route reported here is general and applies to materials beyond Cd_3As_2. The realization of model 2D WSMs may open up many opportunities, including quantized anomalous Hall effects [4], or by serving as a platform for engineering unconventional superconductivity.

*Corresponding author.
stemmer@mrl.ucsb.edu

[1] C. L. Kane and E. J. Mele, Z_2 Topological Order and the Quantum Spin Hall Effect, Phys. Rev. Lett. **95**, 146802 (2005).

[2] B. A. Bernevig, T. L. Hughes, and S. C. Zhang, Quantum spin Hall effect and topological phase transition in HgTe quantum wells, Science **314**, 1757 (2006).

[3] C.-X. Liu, X.-L. Qi, X. Dai, Z. Fang, and S.-C. Zhang, Quantum Anomalous Hall Effect in $Hg_{1-y}Mn_yTe$ Quantum Wells, Phys. Rev. Lett. **101**, 146802 (2008).

[4] S. Sun, H. Weng, and X. Dai, Possible quantization and half-quantization in the anomalous Hall effect caused by in-plane magnetic field, Phys. Rev. B **106**, L241105 (2022).

[5] J.-Y. You, C. Chen, Z. Zhang, X.-L. Sheng, S. A. Yang, and G. Su, Two-dimensional Weyl half-semimetal and tunable quantum anomalous Hall effect, Phys. Rev. B **100**, 064408 (2019).

[6] X. Liu, H.-C. Hsu, and C.-X. Liu, In-Plane Magnetization-Induced Quantum Anomalous Hall Effect, Phys. Rev. Lett. **111**, 086802 (2013).

[7] Y. Zeng, F. Xue, and A. H. MacDonald, In-plane magnetic field induced density wave states near quantum spin Hall phase transitions, Phys. Rev. B **105**, 125102 (2022).

[8] F. Dominguez, B. Scharf, and E. M. Hankiewicz, Crystalline Weyl semimetal phase in quantum spin Hall systems under magnetic fields, SciPost Phys. Core **5**, 024 (2022).

[9] J. Maciejko, T. L. Hughes, and S.-C. Zhang, The quantum spin Hall effect, Annu. Rev. Condens. Matter Phys. **2**, 31 (2010).

[10] M. König, H. Buhmann, L. W. Molenkamp, T. Hughes, C.-X. Liu, X.-L. Qi, and S.-C. Zhang, The quantum spin Hall effect: Theory and experiment, J. Phys. Soc. Jpn. **77**, 031007 (2008).

[11] G. M. Gusev, E. B. Olshanetsky, Z. D. Kvon, O. E. Raichev, N. N. Mikhailov, and S. A. Dvoretsky, Transition from insulating to metallic phase induced by in-plane magnetic field in HgTe quantum wells, Phys. Rev. B **88**, 195305 (2013).

[12] T. Khouri, S. Pezzini, M. Bendias, P. Leubner, U. Zeitler, N. E. Hussey, H. Buhmann, L. W. Molenkamp, M. Titov, and S. Wiedmann, Magnetoresistance in the in-plane magnetic field induced semimetallic phase of inverted HgTe quantum wells, Phys. Rev. B **99**, 075303 (2019).

[13] Y. Xu, G. Jiang, I. Miotkowski, R. R. Biswas, and Y. P. Chen, Tuning Insulator-Semimetal Transitions in 3D Topological Insulator Thin Films by Intersurface Hybridization and In-Plane Magnetic Fields, Phys. Rev. Lett. **123**, 207701 (2019).

[14] O. E. Raichev, Effective Hamiltonian, energy spectrum, and phase transition induced by in-plane magnetic field in symmetric HgTe quantum wells, Phys. Rev. B **85**, 045310 (2012).

[15] M. Kubisa and K. Ryczko, Topological phase transitions and a spin-related metallic state in inverted HgTe quantum wells under in-plane magnetic field, Phys. Rev. B **104**, L161406 (2021).

[16] A. A. Burkov, Quantum anomalies in nodal line semimetals, Phys. Rev. B **97**, 165104 (2018).

[17] A. C. Lygo, B. Guo, A. Rashidi, V. Huang, P. Cuadros-Romero, and S. Stemmer, Two-Dimensional Topological Insulator State in Cadmium Arsenide Thin Films, Phys. Rev. Lett. **130**, 046201 (2023).

[18] Z. J. Wang, H. M. Weng, Q. S. Wu, X. Dai, and Z. Fang, Three-dimensional Dirac semimetal and quantum transport in Cd_3As_2, Phys. Rev. B **88**, 125427 (2013).

[19] J. Cano, B. Bradlyn, Z. Wang, M. Hirschberger, N. P. Ong, and B. A. Bernevig, Chiral anomaly factory: Creating Weyl fermions with a magnetic field, Phys. Rev. B **95**, 161306® (2017).

[20] S. Sun, Z. Song, H. Weng, and X. Dai, Topological metals induced by the Zeeman effect, Phys. Rev. B **101**, 125118 (2020).

[21] Z. Song, S. Sun, Y. Xu, S. Nie, H. Weng, Z. Fang, and X. Dai, First principle calculation of the effective Zeeman's

couplings in topological materials, in *Memorial Volume for Shoucheng Zhang*, edited by B. Lian, C. X. Liu, E. Demler, S. Kivelson, and X. Qi (World Scientific, Singapore, 2021), Chap. 11, pp. 263–281.

[22] T. N. Pardue, M. Goyal, B. Guo, S. Salmani-Rezaie, H. Kim, O. Heinonen, M. D. Johannes, and S. Stemmer, Controlling the symmetry of cadmium arsenide films by epitaxial strain, APL Mater. **9,** 051111 (2021).

[23] J. Ahn and B.-J. Yang, Unconventional Topological Phase Transition in Two-Dimensional Systems with Space-Time Inversion Symmetry, Phys. Rev. Lett. **118,** 156401 (2017).

[24] C. Fang and L. Fu, New classes of three-dimensional topological crystalline insulators: Nonsymmorphic and magnetic, Phys. Rev. B **91,** 161105(R) (2015).

[25] C.-X. Liu, X.-L. Qi, H. J. Zhang, X. Dai, Z. Fang, and S.-C. Zhang, Model Hamiltonian for topological insulators, Phys. Rev. B **82,** 045122 (2010).

[26] P. O. Löwdin, A note on the quantum-mechanical perturbation theory, J. Chem. Phys. **19,** 1396 (1951).

[27] R. Winkler, Quasi-degenerate perturbation theory, in *Spin-Orbit Coupling Effects in Two-Dimensional Electron and Hole Systems*, edited by R. Winkler (Springer, Berlin, 2003), pp. 201–205.

[28] See Supplemental Material at http://link.aps.org/supplemental/10.1103/PhysRevLett.131.046601, which also includes Refs. [29–31], for details on $k \cdot p$ modeling and the in-plane g factor calculations and additional discussions of the results, x-ray characterization, magnetic field alignment procedure, and additional datasets for the 18 nm sample, as well as the temperature dependence of the resistivities at different in-plane magnetic fields.

[29] S. Baidya and D. Vanderbilt, First-principles theory of the Dirac semimetal Cd_3As_2 under Zeeman magnetic field, Phys. Rev. B **102,** 165115 (2020).

[30] R. Xiao, J. Zhang, J. Chamorro, J. Kim, T. M. McQueen, D. Vanderbilt, M. Kayyalha, Y. Li, and N. Samarth, Integer quantum Hall effect and enhanced g factor in quantum-confined Cd_3As_2 films, Phys. Rev. B **106,** L201101 (2022).

[31] L. Fu and C. L. Kane, Topological insulators with inversion symmetry, Phys. Rev. B **76,** 045302 (2007).

[32] F. A. P. Blom, J. W. Cremers, J. J. Neve, and M. J. Gelten, Anisotropy of the electronic g^*-factor in cadmium arsenide, Solid State Commun. **33,** 69 (1980).

[33] S. Jeon, B. B. Zhou, A. Gyenis, B. E. Feldman, I. Kimchi, A. C. Potter, Q. D. Gibson, R. J. Cava, A. Vishwanath, and A. Yazdani, Landau quantization and quasiparticle interference in the three-dimensional Dirac semimetal Cd_3As_2, Nat. Mater. **13,** 851 (2014).

[34] N. P. Armitage, E. J. Mele, and A. Vishwanath, Weyl and Dirac semimetals in three-dimensional solids, Rev. Mod. Phys. **90,** 015001 (2018).

[35] M. N. Ali, Q. Gibson, S. Jeon, B. B. Zhou, A. Yazdani, and R. J. Cava, The crystal and electronic structures of Cd_3As_2, the three-dimensional electronic analogue of graphene, Inorg. Chem. **53,** 4062 (2014).

[36] M. Goyal, S. Salmani-Rezaie, T. N. Pardue, B. H. Guo, D. A. Kealhofer, and S. Stemmer, Carrier mobilities of (001) cadmium arsenide films, APL Mater. **8,** 051106 (2020).

[37] W. Beugeling, Parity symmetry as the origin of 'spin' in the quantum spin Hall effect, Phys. Rev. B **104,** 115428 (2021).

[38] B. Guo, A. C. Lygo, X. Dai, and S. Stemmer, $\nu = 0$ quantum Hall state in a cadmium arsenide thin film, APL Mater. **10,** 091116 (2022).

[39] J. Nilsson, A. H. Castro Neto, F. Guinea, and N. M. R. Peres, Electronic Properties of Graphene Multilayers, Phys. Rev. Lett. **97,** 266801 (2006).

[40] J. Tworzydło, B. Trauzettel, M. Titov, A. Rycerz, and C. W. J. Beenakker, Sub-Poissonian Shot Noise in Graphene, Phys. Rev. Lett. **96,** 246802 (2006).

[41] R. Jackiw, Fractional charge and zero modes for planar systems in a magnetic field, Phys. Rev. D **29,** 2375 (1984).

[42] A. M. J. Schakel, Relativistic quantum Hall effect, Phys. Rev. D **43,** 1428 (1991).

[43] T. Ando, A. B. Fowler, and F. Stern, Electronic properties of two-dimensional systems, Rev. Mod. Phys. **54,** 437 (1982).

[44] M. Shayegan, E. P. D. Poortere, O. Gunawan, Y. P. Shkolnikov, E. Tutuc, and K. Vakili, Two-dimensional electrons occupying multiple valleys in AlAs, Phys. Status Solidi B **243,** 3629 (2006).

[45] Y. Xu, I. Miotkowski, C. Liu, J. F. Tian, H. Nam, N. Alidoust, J. N. Hu, C. K. Shih, M. Z. Hasan, and Y. P. Chen, Observation of topological surface state quantum Hall effect in an intrinsic three-dimensional topological insulator, Nat. Phys. **10,** 956 (2014).

[46] R. Yoshimi, A. Tsukazaki, Y. Kozuka, J. Falson, K. S. Takahashi, J. G. Checkelsky, N. Nagaosa, M. Kawasaki, and Y. Tokura, Quantum Hall effect on top and bottom surface states of topological insulator $(Bi_{1-x}Sb_x)_2Te_3$ films, Nat. Commun. **6,** 6627 (2015).

[47] D. A. Kealhofer, L. Galletti, T. Schumann, A. Suslov, and S. Stemmer, Topological Insulator State and Collapse of the Quantum Hall Effect in a Three-Dimensional Dirac Semimetal Heterojunction, Phys. Rev. X **10,** 011050 (2020).

[48] C. Brüne, C. X. Liu, E. G. Novik, E. M. Hankiewicz, H. Buhmann, Y. L. Chen, X. L. Qi, Z. X. Shen, S. C. Zhang, and L. W. Molenkamp, Quantum Hall Effect from the Topological Surface States of Strained Bulk HgTe, Phys. Rev. Lett. **106,** 126803 (2011).

[49] Y. Xu, I. Miotkowski, and Y. P. Chen, Quantum transport of two-species Dirac fermions in dual-gated three-dimensional topological insulators, Nat. Commun. **7,** 11434 (2016).

[50] S. K. Chong, K. B. Han, T. D. Sparks, and V. V. Deshpande, Tunable Coupling between Surface States of a Three-Dimensional Topological Insulator in the Quantum Hall Regime, Phys. Rev. Lett. **123,** 036804 (2019).

[51] T. Morimoto, A. Furusaki, and N. Nagaosa, Charge and Spin Transport in Edge Channels of a $\nu = 0$ Quantum Hall System on the Surface of Topological Insulators, Phys. Rev. Lett. **114,** 146803 (2015).